Cold Regions Science and Technology 221 (2024) 104175

Contents lists available at ScienceDirect

Cold Regions Science and Technology

journal homepage: www.elsevier.com/locate/coldregions

Influence of the ice shape on ice-structure impact loads

Franciska Müller [a,*], Angelo Böhm [a], Hauke Herrnring [a], Franz von Bock und Polach [a], Sören Ehlers [b]

[a] Institute for Ship Structural Design and Analysis, Hamburg University of Technology, 21073 Hamburg, Germany
[b] German Aerospace Centre (DLR), Institute of Maritime Energy Systems, 21502 Geesthacht, Germany

ARTICLE INFO

Keywords:
Ice-structure interaction
Small scale tests
Crushing
Spalling
Ice shape
Geometry

ABSTRACT

Ships that are navigating in ice covered waters are at risk of colliding with icebergs or ice floes, which can lead to severe damage to the ship's hull in certain conditions. Predicting these loads is of great importance for the design and safety of ships. Ice loads are driven by a range of parameters, including ice properties such as the compressive strength, the geometry of the ship's hull and values related to the interaction (e.g. impact velocity). Classification rules and requirements for polar vessels account for these parameters to a certain extent. However, sea ice exhibits not only variability of its properties but also the geometry of the ice shows a high degree of diversity: icebergs and ice floes exist in multiple different shapes. Therefore, this paper addresses the ice-structure interaction process, focusing on the influence of the initial ice contact shape and its impact on the local load. Additionally, the paper explores the feasibility of pinpointing geometric parameters of the ice responsible for influencing these loads. Ultimately, understanding which ice shape in contact poses the greatest risk would be valuable for improving numerical simulations for the worst case scenario and, consequently, enhancing the safety of ships in ice-prone environments.

To achieve this, a comprehensive drop tower test campaign on a small-scale has been conducted at the test facilities of the Hamburg University of Technology. In these experiments, single impacts of differently shaped ice specimens against a rigid 50 mm steel plate in normal direction were investigated. In the experiments, a drop hammer was released from a predefined drop height to realize a brittle failure of the ice at an interaction velocity of about 2000 mm/s. This falls within the lower range of ship-ice interaction speeds. The drop hammer fell onto the ice specimen which was positioned centered underneath the drop hammer. The investigated specimen geometries were cylindrical shapes of 200 mm diameter with varying caps of cone, dome, wedge, ellipse and other shapes. Overall, 27 different shaped ice specimens were tested. The analysis includes the failure behavior of the ice specimens and the load introduced by the specific contact shapes. Two main failure modes were observed depending on the ice geometry, which showed significant differences in the load magnitude. Further relations between the initial contact area, the cone angle, and the specimen length to the peak force, maximum pressure, and energy were identified.

1. Introduction

According to the latest reports from Allianz Global Corporate and Specialty (AGCS) ice-structure interaction poses a significant risk to shipping operations in the challenging maritime environment of the polar regions (Allianz Global corporate and Specialty (AGCS), 2019; Allianz Global corporate and Specialty (AGCS), 2020; Allianz Global corporate and Specialty (AGCS), 2021). The interaction between vessels and ice formations can lead to detrimental loads on the ship's hull, propellers, and other critical components, potentially resulting in structural damage and operational hazards. One example is one of the latest accidents in March 2023, where the vessel *Yong Xing 56* sank in the Strait of Tartary following damage incurred in a collision with large ice floes (Mike Schuler gCaptain, 2023).

The International Association of Classification Societies (IACS) provides Unified Requirements (UR) for polar-class ships, which play a crucial role in ensuring safe ship designs and operations in ice-covered waters. The design scenario is a glancing impact at the front shoulder

* Corresponding author at: Hamburg University of Technology, Institute of Ship Structural Design and Analysis, Am Schwarzenberg Campus 4 C, 21073 Hamburg, Germany.
E-mail address: franciska.mueller@tuhh.de (F. Müller).

https://doi.org/10.1016/j.coldregions.2024.104175
Received 7 October 2023; Received in revised form 22 January 2024; Accepted 8 March 2024
Available online 15 March 2024

with an angular ice edge using a pressure-area relationship to describe the ice indentation (Daley, 2000). In reality sea ice formations can have a multitude of different shapes that are impacting with the ship's hull, see for example Fig. 1.

Research on the effects of diverse ice shapes in the context of ice-structure interaction is very limited and in most cases this topic is relegated only to a secondary position. Yu et al. (Zhaolong et al., 2021) numerically investigated and showed the influence of different elliptical ice shapes in ice-structure interactions using the elastic-plastic ice material model of Liu et al. (Liu et al., 2011). Habib et al. (Habib et al., 2014) tested twenty-eight (28) truncated ice specimens in small-scale indentation tests to study the compressive failure of poly-crystalline ice during indentation and showed the link between various parameters like cone angle that influence the ice failure processes. They also recommended testing slightly tilted ice specimens to investigate the alignment sensitivity. After the experimental investigation of water, snow, and granular ice effects on ice failure processes and impact loads, Sopper proposed in her dissertation the experimental investigation of more ice geometries (Sopper, 2016). Tuhkuri et al. tested wedge shape ice specimens and observed in the experiments that ice failing in a brittle manner will develop into the shape of a wedge (Tuhkuri et al., 1997) and Dragt and Bruneau (2013) stated that cone shaped ice specimens offer a consistent measure of ice strength in crushing and provides a more analogous crushing or impact scenario to real-life interactions (Dragt and Bruneau, 2013; Bruneau et al., 2013).

These studies suggest a geometric influence, but a thorough quantification of this influence is missing. We conducted a comprehensive drop tower test campaign to bridge this knowledge gap with 27 different ice specimen shapes. The idealized shapes are chosen to investigate the influence of the initial contact form (point-like, line-like and area-like), the initial contact size, as well as the influence of the specimen shape on the failure behavior and to establish a correlation between geometric parameters, load measurements, and failure behavior. All ice specimens investigated are cylinders with different shaped caps. The experiments include truncated cones, shortened specimens, elliptical and wedge shape specimens, other special geometries, and inclined ice cylinders to investigate the alignment sensitivity. The central research questions are: Does the ice shape in contact influence the load, and if so, how significant is it? Which ice geometry parameters are crucial in determining the magnitude of the load and, therefore, define the most detrimental ice shape in contact among those investigated? Ultimately, this analysis can aid in numerical simulations of ship impacts in ice-prone regions, using the most detrimental ice shape for assessing ship structures.

Fig. 1. A ship's hull interacting with a multitude of different ice shapes. Highlighted in red are examples of varying geometric shapes, including a wedge shaped centrally positioned, a conical form proximal to the ship's hull, and a rounded contour located to the right. Photo source: Franz von Bock und Polach.

2. Experiments

This chapter describes the ice specimen production and preparation, the experimental setup and the test matrix.

2.1. Specimen production and preparation

The ice specimen production process is well established in the *Institute of Ship Structural Design and Analysis* of the *Hamburg University of Technology* (Soares and Garbatov, 2017; Herrnring et al., 2020; Böhm et al., 2022; Müller et al., 2023) and is based on Gudimetla et al. (Reddy Gudimetla et al., 2012). However, instead of self-made crushed ice, commercial crushed ice was used. The ice specimens were prepared and frozen at -10°C. Further, the raw specimens were cylindrical, with a diameter of 200 mm and a height of 200 mm, except for the shortened specimens. PVC-U pipes with an inner diameter of 200 mm, closed at the

Fig. 2. PVC-U pipe filled with crushed ice and distilled water.

bottom with a thin metal plate ensuring good heat conduction, were filled with one-third distilled water and two-thirds crushed ice, see Fig. 2. For insulation, the pipes were covered with a polystyrene lid to ensure the freezing from bottom to top and to avoid cracking during the freezing time of about 4 days. After the freezing process, the mold was removed under the ambient lab-temperature of around 20°C. The preparation of the final specimen shapes took place in a refrigerated container at −10°C with an ice sharpener for the rotational symmetric forms (cone, truncated cone, ellipse, sphere, cone with sphere tip) and and a semi-automatic band-saw for the other forms (wedge, pyramid, inclined cylinder).

2.2. Experimental setup

The experiments were conducted at the *Institute of Ship Structural Design and Analysis* laboratory at the *Hamburg University of Technology* on a drop tower to realize high interaction velocities, see Fig. 3.

The drop tower experiment, displayed in Fig. 3, is energy limited compared to a compression test with a hydraulic cylinder. The weight of the drop hammer was 218 kg, and all tests were conducted at an interaction velocity of 2.0 m/s, with maximum deviations of +0.16 m/s and − 0.225 m/s. An emergency release hook released the vertically guided drop hammer crushing the ice specimen. The specimen was placed on the center of the measuring platform, supported in a specimen hold underneath the drop hammer. The ice specimen is confined by the specimen hold from the bottom to 50 mm. The laser displacement sensor measured the movement of the drop hammer during the experiment, and four strain gauge-based load cells of the type *Sartorius PR 6251/14 PanCake Level Sensor* measured the impact load, which were connected to the base plate, see Fig. 4. The selected load cells, as specified by the manufacturer with accordance to VDI / VDE 2637, exhibit minimal elastic deformation (< 0.5 mm under a nominal load of 10 t) and low hysteresis (< 0.15% C_n), ensuring accurate force measurements. These characteristics minimize structural deformations within the load cells and maintain consistent measurements, thereby supporting the reliability and precision of the presented results. The displacement and load signals were measured at a sampling rate of 100 kHz. Later in Fig. 9, the measurement resolution is illustrated. Between points a and c around 140 data points are captured, highlighting the level of detail of the measurement system during the impact phase. A high-speed camera recorded pictures of the failure behavior of the specimens with up to 2300 frames per second. Shock dampers were utilized to protect the load cells by absorbing the residual energy of the drop hammer after the crushing of the specimen.

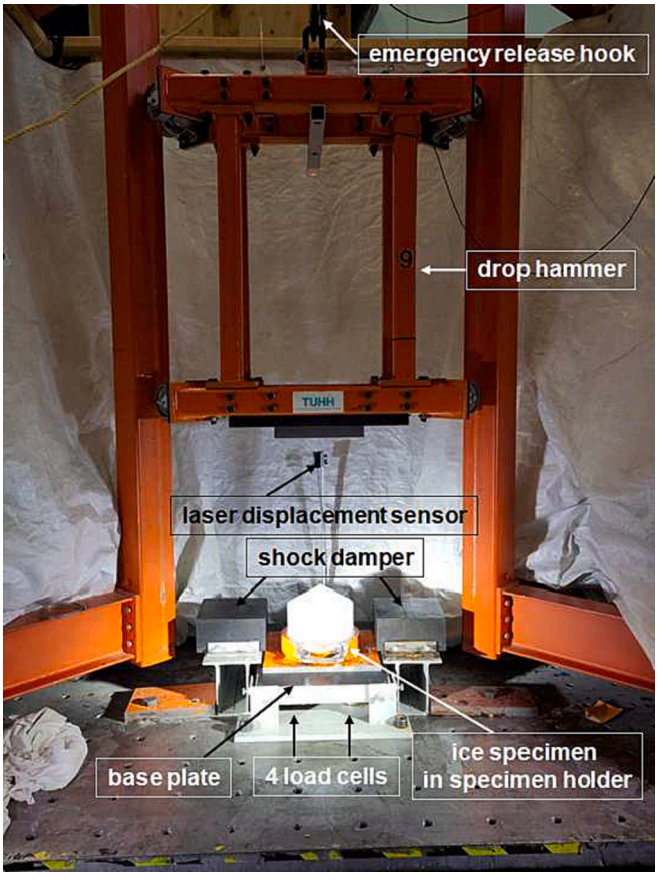

Fig. 3. Drop tower at the Institute of Ship Structural Design and Analysis of the Hamburg University of Technology.

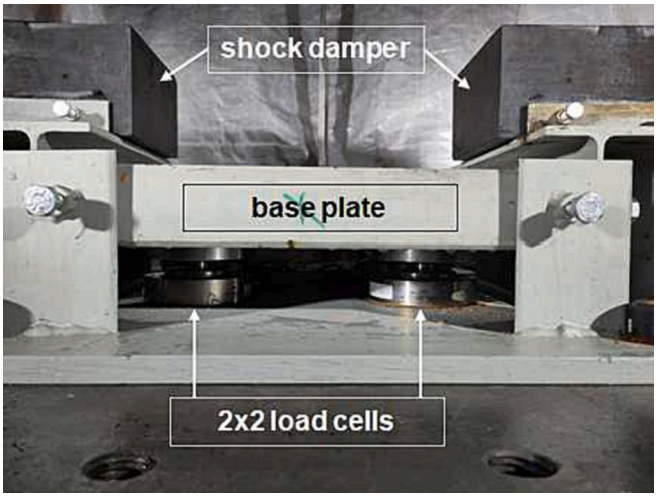

Fig. 4. Close up of the base plate with four load cells underneath, two in the front and two in the back.

2.3. Test matrix

Four test series, including in total 27 different ice specimen shapes, were conducted to investigate the influence of different geometry parameters on the measured impact load. Each test was repeated at least three times.

1. **Truncated cone**: This test series included cones, truncated cones with three different cone angles (10, 20, and 30°) and truncation diameter (50, 100, and 150 mm), and a cylindrical specimen. This test series has 13 different specimen geometries; see Fig. 5. The height of all specimens is 200 mm. This test series analyzed the influence of the cone angle and the initial contact area on contact force and failure mode.
2. **Shortened specimen**: Three different geometries of the test series *truncated cone* (cone, truncated cone, and cylinder) were tested for three different specimen heights. With this test series, the influence of the specimen length was analyzed; see also Fig. 5a. The cone and the truncated cone had a cone angle of 30° and a truncation diameter of 100 mm.
3. **Inclined cylinder**: Cylinders with inclined top surfaces had 1°, 5°, and 10° of inclination (Fig. 5b).
4. **Special geometries**: In this test series, the dome-shaped specimen, Fig. 5c, the elliptical specimen, Fig. 5d, the conical specimen with dome-shaped tip Fig. 5e, the pyramidal specimen with four side faces Fig. 5f, and the wedge shaped specimen Fig. 5g, were analyzed.

3. Results

This section covers the analysis of recorded data, the shape specific failure behavior as well as its impact on interaction force, pressure and

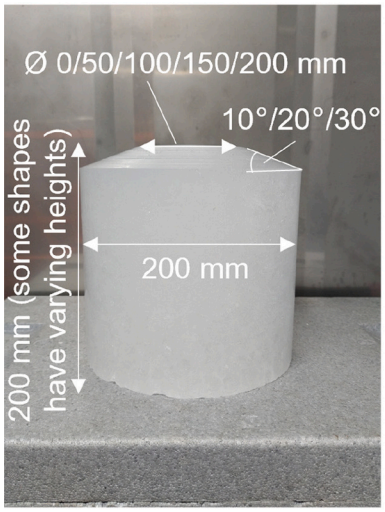

(a) Cones, truncated cones and cylinder

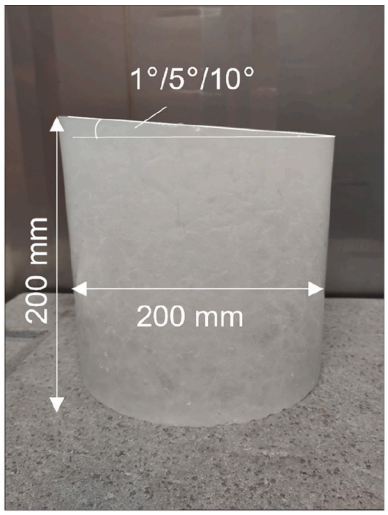

(b) Inclined cylinder

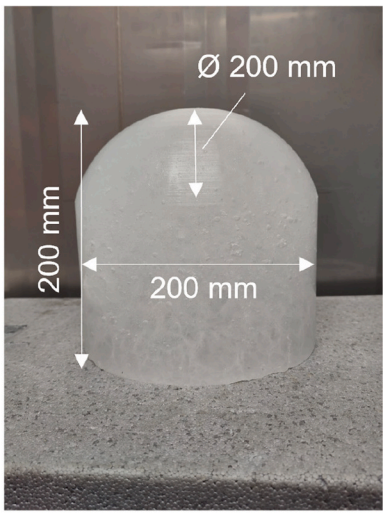

(c) Dome-shaped specimen

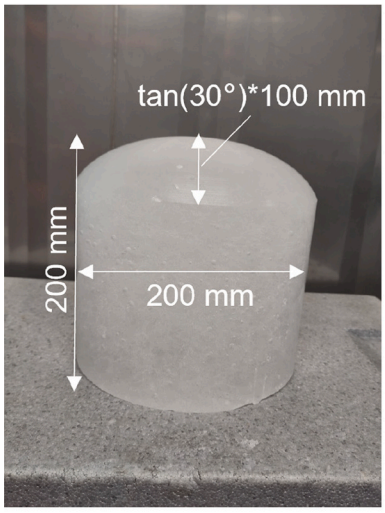

(d) Elliptical specimen

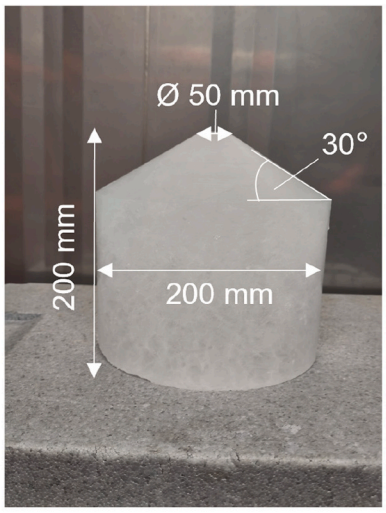

(e) Conical specimen with dome-shaped tip

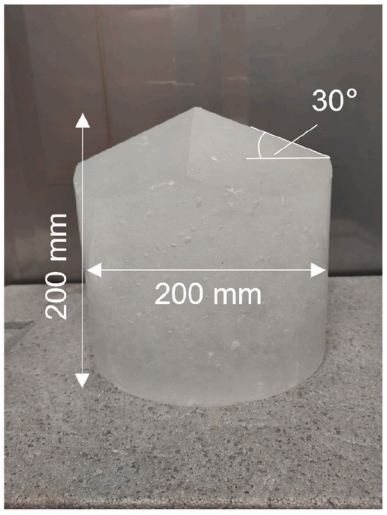

(f) Pyramidal specimen with four side faces

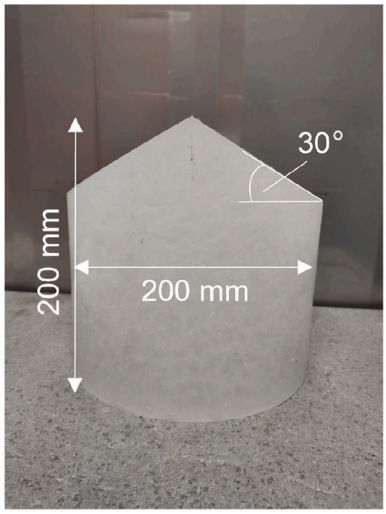

(g) Wedge shaped specimen

Fig. 5. Dimensions of the tested specimen shapes.

energy.

3.1. Data analysis

The preparation of the data analysis included automatic summing up of all load-cell signals to the total force and cropping the data to the relevant range. In the signal three time steps were automatically identified with a script, which are shown in Fig. 6: the start of impact (t1), the point of maximum force (t2), and the endpoint of the impact (t3). For t1, a threshold of 0.5 kN was established to define the start of impact. t2 was identified by taking the maximum value of the force signal. For t3, a threshold of 99.9% of the maximum displacement was defined as the endpoint of the impact to neglect noise peaks. The parameters extracted are the maximum force (f_{peak}) and the maximum nominal pressure (p_{max}). Furthermore the energy (E_{t2}) that is transferred from the drop hammer through the ice to the load cells until the maximum force is reached as well as this energy in relation to the crushed volume (E_{cV}) is analyzed. The maximum force is the force value at t2. Eq. (1) is the formula of the maximum nominal pressure. In the experiments, pressure measurements were not recorded. Therefore, in this paper, references to pressure pertain to nominal pressure.

$$p_{max} = max(p(z)) \tag{1}$$

where $p(z)$ is the nominal pressure over displacement curve, which is calculated with:

$$p(z) = \frac{f(z)}{a_{geo}(z)} \tag{2}$$

Here $f(z)$ is the force over displacement curve and $a_{geo}(z)$ is the curve of the nominal contact area between the ice and the plate over the displacement. The function of the contact area is individual for every ice shape and changes over height of the specimen. The equation used to calculate the normalized initial contact area, which will be employed in subsequent diagrams within this paper, is as follows:

$$a_{n,geo} = \frac{a_{geo}}{\pi \cdot r_{cyl}^2} \tag{3}$$

where a_{geo} is the initial contact area at the specimens top surface (individual for every specimen shape) and r_{cyl} is the radius of the base cylinder portion of the specimen, which has a fixed value of 100 mm for all specimen shapes. The energy (E_{t2}) is taken as the area under the force vs. displacement curve (f(z)) from the start of the impact force (t1) until the maximum force value (t2) is reached, presented in Eq. (4). The energy is assumed to be a measure of the energy absorbed by the ice until it globally fails. This method enables the treatment of all test runs using the same automated script and facilitating direct comparison between them.

$$E_{t2} = \int_{z(t1)}^{z(t2)} f(z)\,dz \tag{4}$$

The Energy per crushed volume is calculated with the following formula:

$$E_{cV} = \frac{E_{t2}}{V_{geo,t2}} \tag{5}$$

where $V_{geo,t2}$ is the volume of the crushed volume calculated by following formula:

$$V_{geo,t2} = V_{geo}(z(t2) - z(t1)) \tag{6}$$

$V_{geo}(z)$ is the function of the ice specimen volume which changes over height and is individual for each of the ice shapes.

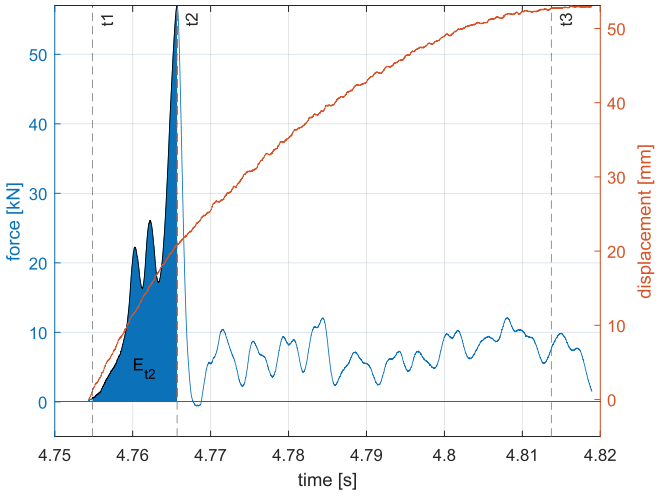

Fig. 6. Example of the analysis of test data from test run two of a conical specimen with 30 cone angle.

3.2. Shape dependent failure behavior

The failure behavior of each specimen geometry was analyzed. This was done to identify correlations between failure behavior and force, energy, and pressure. In the following, we distinguish between specimens with a point-like, a line-line, and an area-like initial contact area. The initial contact area is the area of the specimen that is touched by the drop hammer at first contact. Specimens classified with a point-like initial contact area are cones, rounded cones, dome-shaped, ellipse-shaped, and pyramidal specimens. The wedge-shaped specimen is the only specimen with a line-like initial contact area. Specimens with an area-like initial contact area are cylinders and truncated cones. Furthermore, it is differentiated between the local and global failure of ice specimens. The local failure describes a crushing event with spacial concentration limited to the top of the specimen while the rest of the specimen stays intact. Local failure occurs before the maximum load is reached and is reflected by local peaks. A global failure refers to cracking or a global spalling event that shows fractures throughout the entire specimen and is accompanied by a significant drop in force once the global maximum force is reached. The following describes two exemplary test cases showing two different failure behaviors. Other test cases can be found in the appendix 10.1, 10.2 and 10.3.

3.2.1. Example 1 - local failure followed by global failure

Example 1 is a test run of a specimen with a pyramidal shape with a point-like initial contact area. Fig. 7 shows the force-displacement curve of this test run. Three points (‘a’, ‘b’ and ‘c’) are highlighted in red, marking the positions of the high-speed footage shown in Fig. 8. In Fig. 8a, the specimen is intact just before the contact with the drop hammer. Fig. 8b shows a local failure by crushing at the tip of the specimen. This is in the uprising portion of the load signal. The maximum force of 40.9 kN is reached after a displacement of the drop hammer into the specimen of 14.3 mm. After that, the global failure of the specimen appears with a crack that runs through the specimen, as shown in Fig. 8c. This failure is going along with an instant drop in load. The same failure behavior characterized by an initial local failure by crushing followed by a global failure in the form of spalling is observed for specimens with a cone shape, rounded cone shape, inclined cylinder or a wedge shape. The wedge shaped specimen is the only shape with a line-like initial contact area. Therefore, the high-speed footage and force vs. displacement plot of the wedge shape specimen is given in the appendix 10.1. The wedge-shaped specimen initially undergoes a phase of initial crushing along the upper edge. Following this, spalls begin to form from the upper edge, moving in circular patterns towards the vertical side. Eventually, axial cracks emerge, extending through the entire ice specimen and leading to spalling towards the inclined sides.

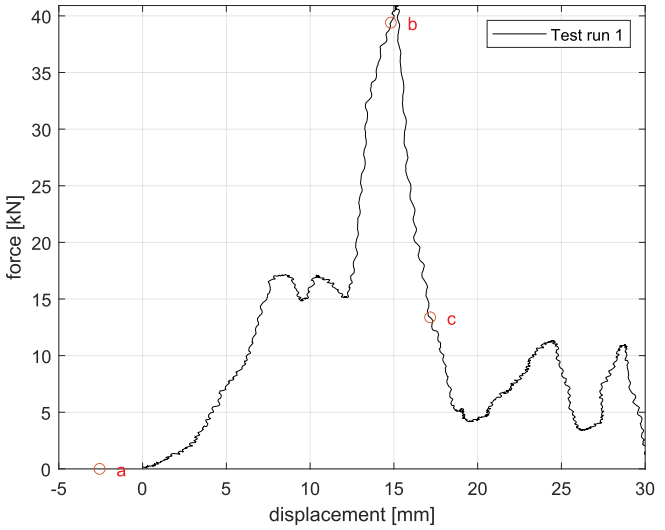

Fig. 7. Force vs. displacement plot of test run 1 of a pyramidal shaped ice specimen. The red circles mark the positions of high speed footage in Fig. 8. a: before impact; b: building up of load while local crushing of the tip of the specimen; c: global failure of ice specimen accompanied with a significant drop in load. (For interpretation of the references to colour in this figure legend, the reader is referred to the web version of this article.)

Further, the same data (force-displacement curve and high speed footage) are given for the inclined cylinder with an inclination of 10°. In this scenario, the drop hammer initially contacts the edge of the specimen, given its elevated position, contrary to other shapes where the center of the specimen is the initial impact point. Failure begins with a phase of crushing along the higher edge, succeeded by spalling towards the side of the higher edge. As the drop hammer progresses past the specimen's center, spalling initiates towards the opposite side with the lower edge.

3.2.2. *Example 2 - instant global failure*

Example 2 is the test run of a specimen in shape of a truncated cone with an area-like initial contact area. This truncated cone has an upper diameter of 100 mm and a cone angle of 30 to the horizontal. Fig. 9 presents the force-displacement curve of one test run with the above described truncated cone. Three positions are marked with 'a', 'b' and 'c', indicating the points of the high-speed footage showed in Fig. 10. For this specimen, one single high load peak is observed. Fig. 10a shows the intact specimen shape before the contact with the drop hammer. After that, cracks occur in the whole specimen body, see Fig. 10b. The peak load is reached in 1.4 mm displacement of the drop hammer into the ice specimen with a magnitude of 124.9 kN. After that, the load drops because of the global failure of the specimen, as shown in Fig. 10c. The same failure behavior characterized by an instant global failure of the specimen with no or only little crushing is observed for all other specimens with an area-like initial contact area (truncated cones and cylinder) and for the dome and elliptical shaped ice specimens. As the dome and elliptical specimen have a point-like initial contact area and therefore differ in shape significantly from the one shown here, the failure behavior of an elliptical specimen is shown in the appendix 10.3 together with the force-displacement plot of one test run. Upon contact with the drop hammer, axial cracks swiftly propagate throughout the entire body of the specimen, leading to the formation of substantial spalls detaching from the specimen.

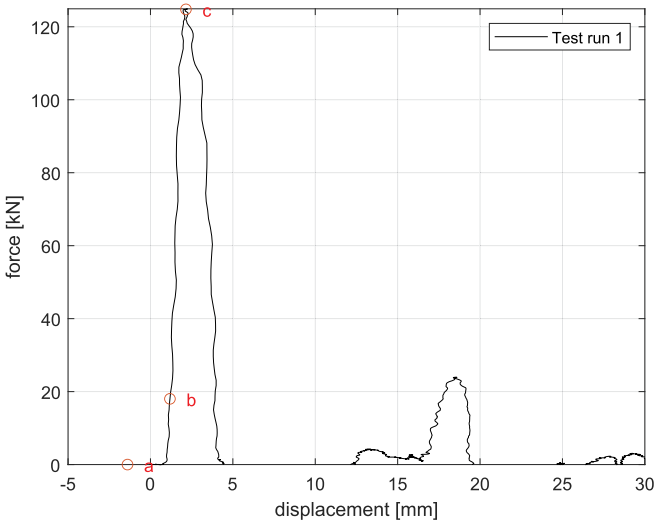

Fig. 9. Force vs. displacement plot of test run 1 of truncated cone ice specimen. The red circles mark the positions of high speed footage in Fig. 10. a: before impact; b: building up of load while cracks develope; c: global failure of ice specimen accompanied with a significant drop in load. (For interpretation of the references to colour in this figure legend, the reader is referred to the web version of this article.)

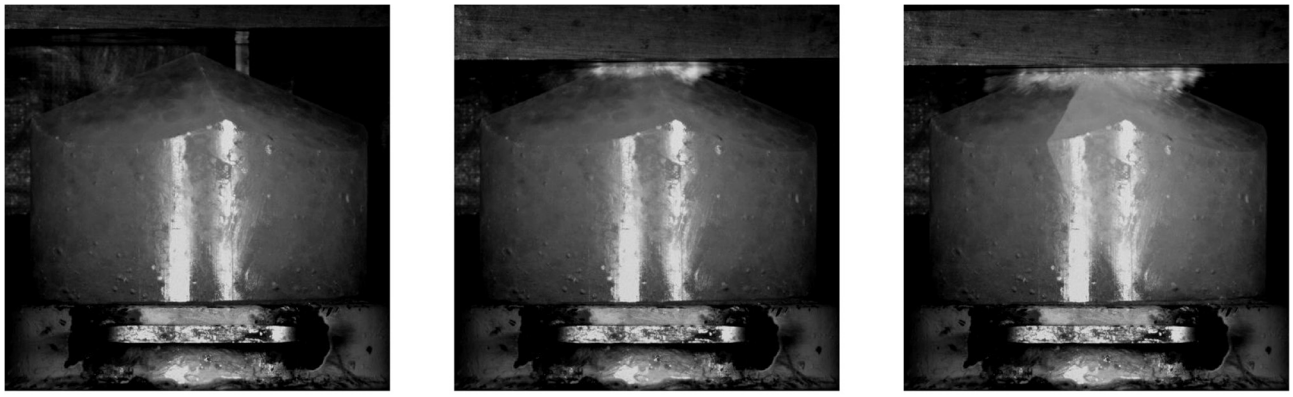

(a) intact ice specimen before contact

(b) local crushing at tip of the ice specimen

(c) global failure of the ice specimen by cracking

Fig. 8. Failure behavior of an ice specimen with pyramidal form. The conical ice specimens and the cone shaped ice specimen with a round tip showed a similar failure behavior.

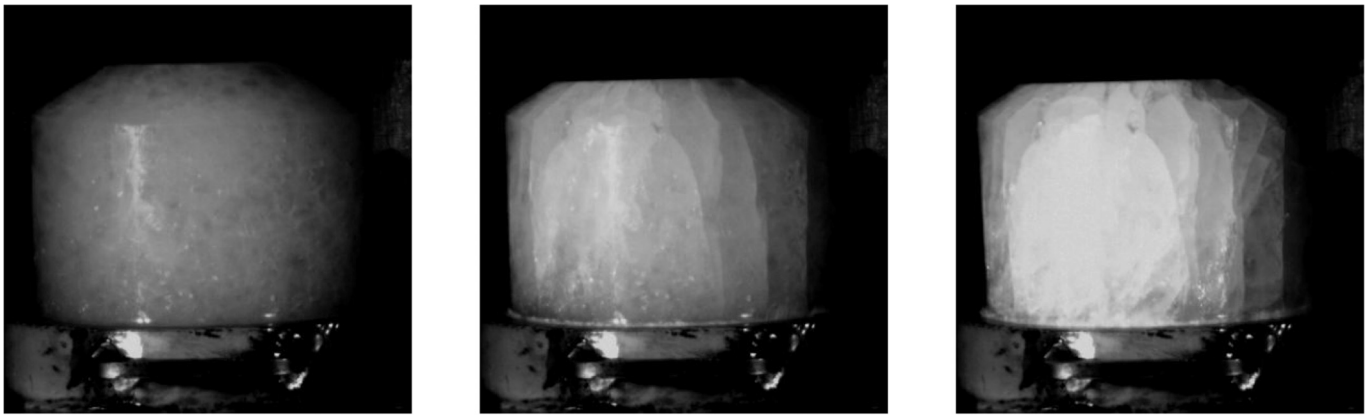

(a) intact ice specimen before contact

(b) initial failure at first contact by cracks propagating downwards

(c) global failure of ice specimen by cracking

Fig. 10. Failure behavior of a truncated cone ice specimen with 30° cone angle and 100 mm upper diameter. Ice specimens with truncated cone shape at different cone angles and upper diameters showed similar failure behavior.

3.3. Analysis

In this section, the failure behavior described in the section above is correlated to the measured peak load, maximum pressure and energy until peak load. Fig. 11 shows f_{peak} in relation to E_{t2}. Two different groups of specimens are identified depending on the failure behavior. The red markers in Fig. 11 refer to those specimens that show instant global failure. These specimens have an area-like contact area (truncated cone and cylinder) or a rounded contact shape like the dome and elliptical specimen (Fig. 5c and d). The black markers refer to specimens that experience initial local crushing before the global failure arises. These are specimens with a point-like initial contact area (except for dome and elliptical shaped specimens) and specimens with a line-like initial contact area (wedge shaped specimen). An indication of the dominating failure behavior is the displacement that the drop hammer covers between first contact with the ice specimen and the maximum force. In our experiments all specimens with a displacement of 3.5 mm or less (red markers) show instant global failure and reach forces between 30 kN and 400 kN. The energy (E_{t2}) which the ice absorbs until the maximum force is reached of these specimens has a positive linear relation to the peak force with values up to 400 J. Specimens that show a displacement of more than 3.5 mm (black markers) first show a local failure by a distinct period of crushing at the tip of the specimen before a spalling or cracking event causes a global failure of the ice specimen. These ice geometries have peak loads below 75 kN, but show the absorption of significant energy levels, with values ranging from 75 J to over 450 J.

The analysis in Fig. 11 is independent to the shape of the specimens, which is addressed next.

3.3.1. Initial contact area

Fig. 12 shows the peak force for selected specimen geometries sorted by magnitude. This diagram shows that ice shapes with an area-like initial contact area have, on average, a lot higher peak force than specimens with a point- or line-like initial contact area. The first four specimens have an area-like initial contact area, showing force values above 100 kN. This is followed by the 1° inclined cylinder, which is on

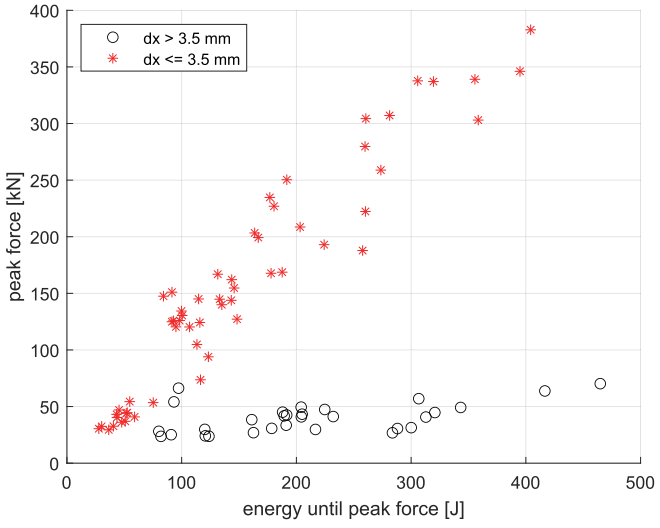

Fig. 11. Peak force (f_{peak}) over energy until peak force (E_{t2}) for specimens that show first local crushing in black (dx > 3.5 mm) and specimens that show immediate global failure in red (dx ≤ 3.5 mm). (For interpretation of the references to colour in this figure legend, the reader is referred to the web version of this article.)

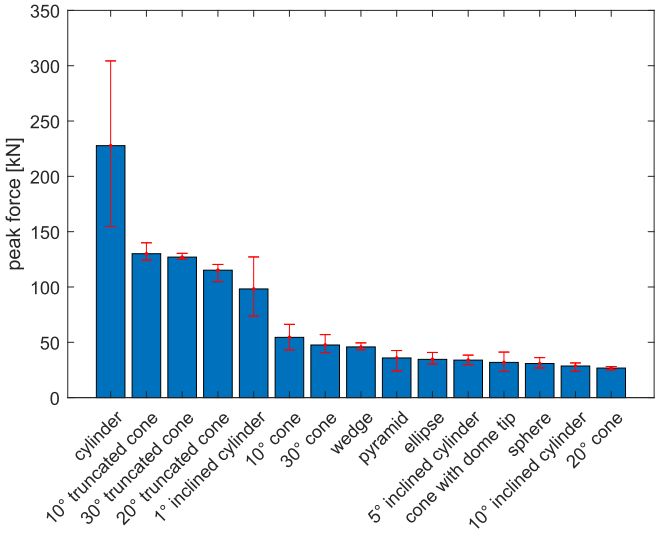

Fig. 12. Peak forces (f_{peak}) of selected ice specimen geometries. The blue bars show the mean peak force value of the test runs of each specimen geometry and the red lines show the maximum and minimum values of the peak force for each geometry. (For interpretation of the references to colour in this figure legend, the reader is referred to the web version of this article.)

the edge between area-like and point- or line-like initial contact area specimens. All following geometries have a point or line-like initial contact area.

In the test series 'truncated cone', illustrated in Fig. 13, the initial contact area of the ice specimens was varied. The diameter of the initial contact areas was 50 mm, 100 mm, 150 mm and 200 mm. The first three are truncated cones and the last one is a cylinder with a normalized initial contact area of 1. Fig. 14a shows the trend of the peak force depending on the initial contact area. The peak force increases with increasing initial contact area independent of the cone angle. The only exception is the 150 mm truncated cone of the 30° series. This shows a higher value than the cylinder. Further, an increase in the scatter of the data points can be seen for higher initial contact areas. The same trend is seen with the energy, see Fig. 14b. The maximum pressure shows an opposite trend with decreasing values for increasing initial contact area, as shown in Fig. 15a.

Potentially, a misalignment between the upper specimen surface and the drop hammer plate causes the data to scatter. The misalignment might be due to inaccuracies in specimen production and minor rotation of the drop hammer, which both lie in a range of ± 0.5°. Furthermore, investigations with cylindrical specimens that have an inclined top surface of 1, 5 and 10° showed that already small angles entail a significant drop in load. Fig. 15b shows this effect. The load decreases with increasing inclination angle. The reduction in load within the small angle range of 0 to 1° is quite substantial, showing a mean load drop of approximately 130 kN. However, in the larger angle range of 5 to 10°, the load decrease insignificant with a value of around 5 kN.

3.3.2. Cone angle

Further, the influence of the cone angle was analyzed. This was done for conical specimens and the three different truncated cone specimens (small, medium, and large). Small is a truncated cone with an upper diameter of 50 mm, medium with 100 mm and large with 150 mm, like shown in Fig. 13. The angles that were investigated were 10, 20 and 30° to the horizontal. Fig. 16a shows the peak force over the cone angle for the four mentioned geometries. No clear trend depending on the cone angle can be identified. Only for the largest truncated cone the peak force increases with increasing cone angle. When looking at the energy per crushed volume, a clear trend can be identified: The sharper the cone, the less energy is needed to crush the tip of the specimen, as shown in Fig. 16b. The influence of the cone angle on the maximum pressure for truncated cones show that the pressure increases with increasing cone angle. This is shown in Fig. 17.

3.4. Specimen length

In a next step the influence of the specimen length was investigated for three different geometries: cylinder, truncated cone (30°/100 mm upper diameter) and cone (30°). The longest specimen measured 200 mm, while the shorter versions the cylindrical part trimmed to 100 and 50 mm. In the shortest version, only the cap was protruding from the specimen holder. The specimen length is also a measure for the confinement of the specimen. The shorter the specimen, the more confined is it due to the specimen holder. (Herrnring et al., 2020) defined the confinement with the ratio G/D, were G is the gap height between specimen hold and interacting plate and D the specimen diameter. Fig. 18a shows the peak force values over the specimen length for three different geometries. The results are inconclusive. No significant trend that applies to all three specimen shapes can be observed. Only for the cylindrical specimen a slight trend for the peak force to decrease with the specimen length is observed, yet the data exhibits considerable scatter. The data indicates that the shape of the ice specimen has a more significant impact on the peak force than the length of the specimen. The maximum variation of the mean loads caused by different length of the specimens is found for the cylindrical specimen shape with around 70 kN. However the variation of the mean load for the 200 mm specimens for different shapes lies between 80 and 180 kN. In the analysis of the energy in Fig. 18b only the truncated cone shows a decreasing trend with increasing specimen length. The other geometries have such a high scatter that no trend can be identified. The maximum pressure presented in Fig. 19 shows for the cylindrical and the truncated cone shape a tendency to increase with decreasing specimen length.

4. Discussion

The experiments presented in this paper provide a more profound insight into how the initial ice contact shape influences the load in an ice impact scenario involving a rigid structure. The analysis presented underscores a significant dependency between the specimen's geometry and the ice load.

Specimens with a parallel contact condition at first contact show higher loads than specimens with a pointed or non area-like initial contact shape. However, an ideal parallel contact scenario is a conservative case as actual ship-ice interactions seldom exhibit such conditions due to the curved ship hull and the highly irregular ice floe shapes as shown in Fig. 1.

Two main failure behaviors were observed, categorizing specimens into two groups based on the ice shape, each assigned to one of these behaviors. The displacement of the drop hammer into the ice specimen at the point of the maximum load was found as an indicator for the dominating failure mode. A small displacement indicated an instant global failure of the specimen by spalling. This was characteristic for ice contact shapes with either a flat or rounded contact surface. A larger displacement indicated a period of local crushing at the tip of the specimen while the rest of the specimen stayed intact. The global failure, by a vertical crack or spalling event, occurred afterwards. The magnitude of the peak force and the absorbed energy, until the peak force is reached, is governed by the failure behavior. In case of an instant global failure, the peak force reaches values up to 400 kN for cylindrical specimens. The peak force for cases that include initial local crushing does not exceed 75 kN. The latter is assumed to be caused by the high energy consumption in the crushing process. However, there could be

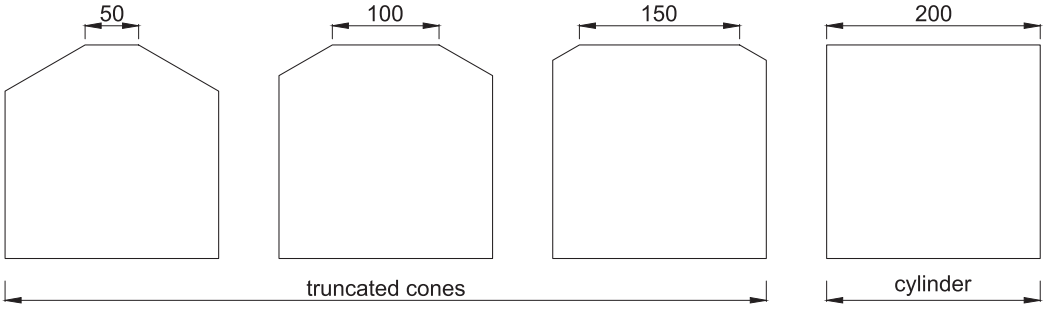

Fig. 13. Truncated cone series with 30° cone angle without the conical ice specimen. Going from left to right the size of the initial contact area increases.

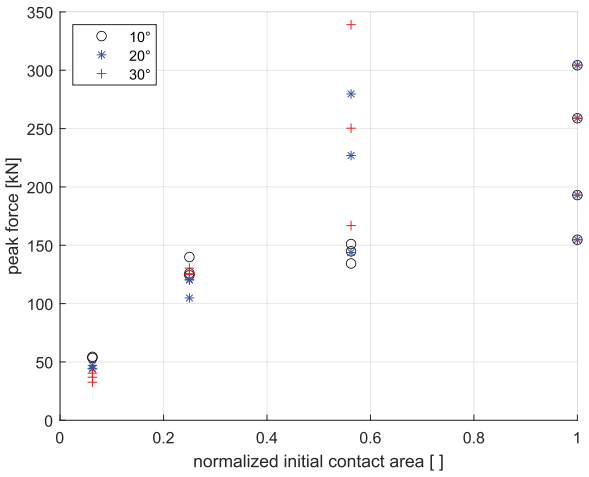

(a) Influence of normalized initial contact area ($a_{n,geo}$) on peak force (f_{peak})

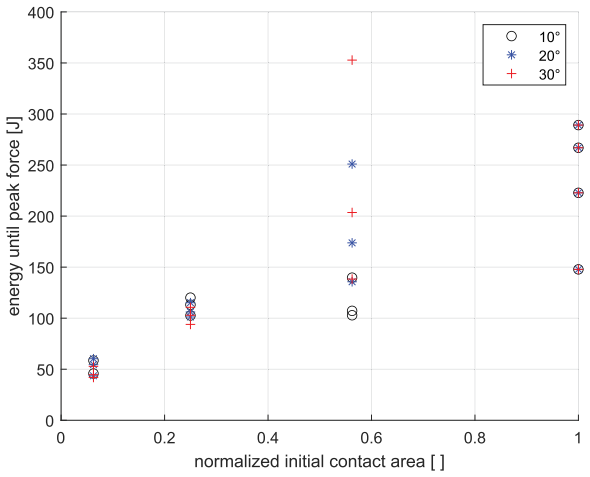

(b) Influence of normalized initial contact area ($a_{n,geo}$) on energy until peak force (E_{t2})

Fig. 14. Truncated cone series: peak force and energy dependency on initial contact area.

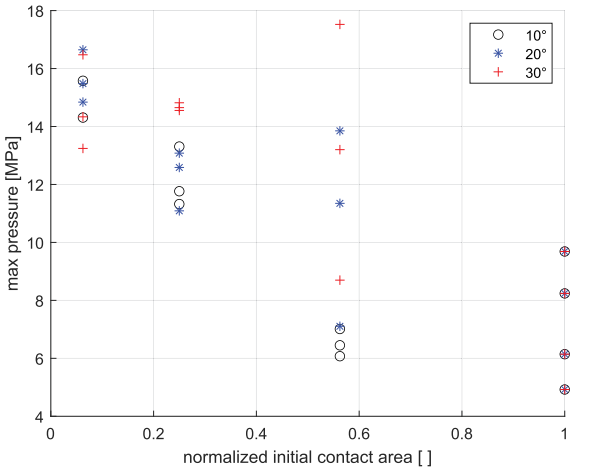

(a) Influence of normalized initial contact area ($a_{n,geo}$) on maximum pressure

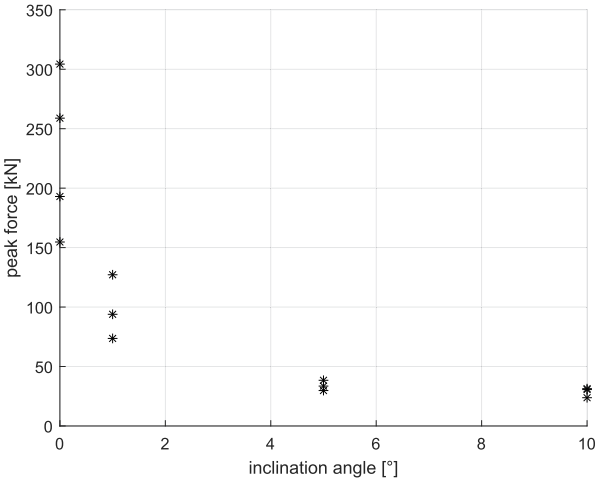

(b) Influence of inclination angle on peak force (f_{peak})

Fig. 15. left: pressure at peak force for truncated cone series; right: peak force for inclined cylinder series.

minor inaccuracies in the experiments arising from the production of ice specimens and the experimental setup. These could affect the precision of the pressure and contact area results, which is quantified below. Three potential sources of inaccuracies are considered:

- The top surface of the ice specimens (cylinder and truncated cone) might not be perfectly parallel due to the precision of the bandsaw. A maximum angular deviation of 0.5° is possible, leading to a deviation in contact area of maximally 0.3%. For the purpose of this study this can be neglected. However, the misalignment might contribute to the scatter in peak force data due to the change in failure mode, like shown in 15b.
- The elastic deformation of the drop hammer during impact can cause a difference in displacement measurement, resulting in an estimated maximum deviation of 5% in contact area and nominal pressure for the worst case. This would apply to the conical specimen with a cone angle of 10° while it would be less for other specimens.
- There is a possibility of the drop hammer rotating during impact, up to 0.5°, which can cause a deviation in the calculated contact area. This becomes particularly relevant for the conical ice specimens, as they fail after a period of crushing where the displacement of the drop hammer is used to calculate the nominal contact area. In this case, the deviation can be quite significant, with values over 50%. Consequently, the conical specimens are excluded from the pressure diagrams. It is important to note that the cylindrical and truncated cone specimens fail upon first contact, when the drop hammer hits the top surface. In this case, a meaningful contact pressure can be determined.

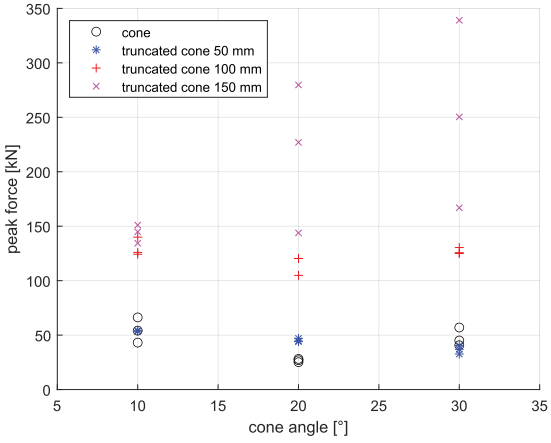

(a) Influence of cone angle on peak force (f_{peak})

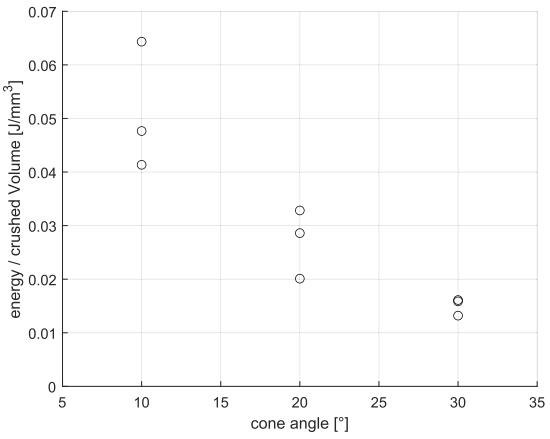

(b) Energy per crushed volume (E_{cV}) for cones of different angle

Fig. 16. Truncated cone series: peak force and energy dependency on cone angle.

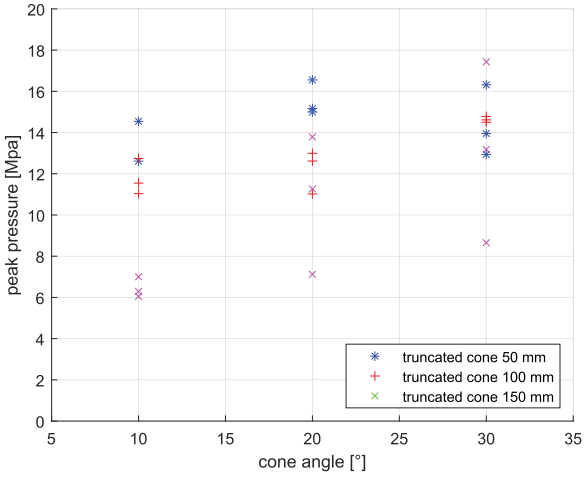

Fig. 17. Influence of cone angle on maximum pressure (p_{max}).

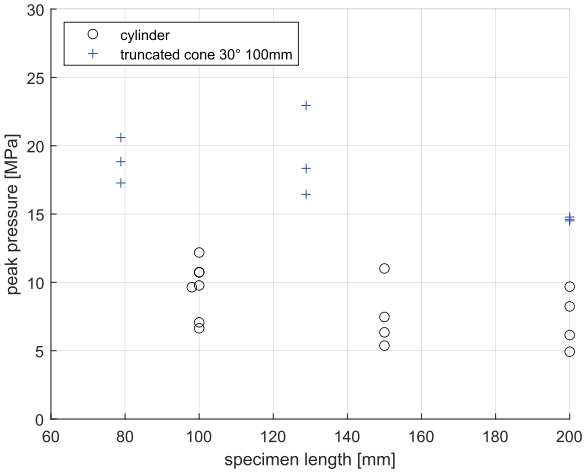

Fig. 19. Influence of specimen length on maximum pressure (p_{max}).

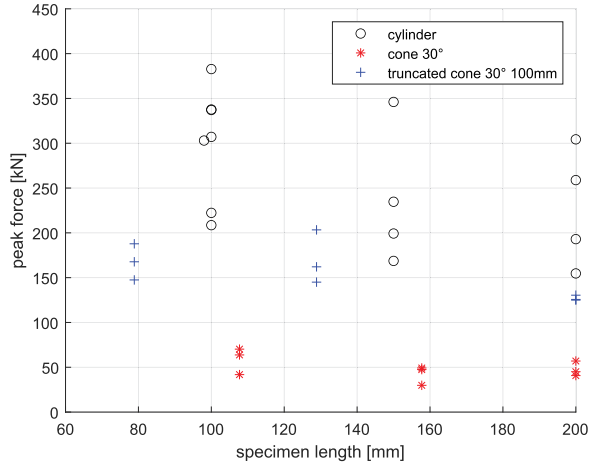

(a) Influence of specimen length on peak force (f_{peak})

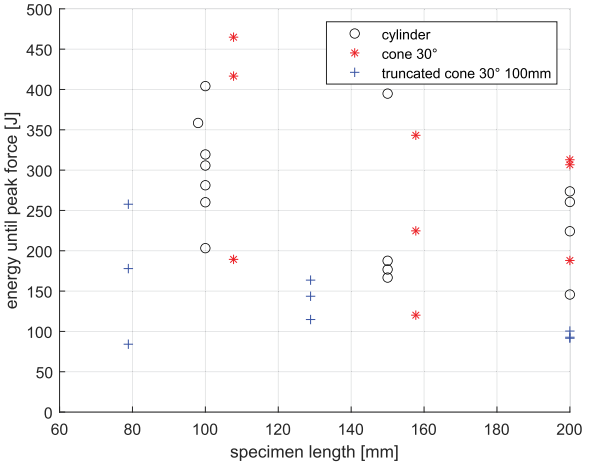

(b) Influence of specimen length on energy until peak force (E_{t2})

Fig. 18. Shortened specimen series: peak force and energy dependency on specimen length.

Furthermore, the influence of a parametric change of the initial contact area, the cone angle and the specimen length were analyzed. The size of the initial contact area turned out to be a dominating parameter for the magnitude of the measured load. The load increases with increasing initial contact area. Furthermore, it was shown that a misalignment between the ice top surface and the drop hammer plate results in a significant drop in load already for a small angle of 1° to the horizontal. This leads to a high scatter in the data of the experiments with specimens of a great initial contact area, like a cylindrical specimen. This must be considered in future experiments investigating an ideal parallel impact condition between structure and ice. A high number of test runs for those ice shapes is recommended, or an adjustment of the test setup to prevent misalignments.

The cone angle was found to have no or only little influence on the peak force for the tested geometries. This is in line with the findings of Herrnring et al. (Herrnring et al., 2020). They investigated the confinement effect in ice extrusion tests and tested conical specimens of 10, 20 and 30° at 10 mm/s among other. They found no significant influence of the cone angle on the maximum force. In the present experiments, only the truncated cone with an upper diameter of 150 mm showed increasing peak forces with increasing cone angle. Habib et el. (Habib et al., 2014) found decreasing forces with steeper cone angles. The experiments for conical specimens showed further that the energy per crushed volume decreases the sharper the cone is. Further the truncated cone specimens showed an increase in maximum pressure with cone angle. Habib et al. (Habib et al., 2014) found for conical specimens with a truncated tip an decrease in pressure with steeper cone angle.

The influence of the length of the ice specimen was insignificant. The tested specimens had an G/D ratio between 0.14 and 0.75. Also Herrnring et al. (Herrnring et al., 2020) found for G/D ratios above 0.25 for conical specimens at an impact velocity of 10 mm/s no impact on the load magnitude. In the present experiments, only the cylindrical shaped ice specimen showed a decreasing peak load with increasing specimen length.

5. Conclusion

In this paper, we were addressing the question if the shape of the ice has an influence on the load magnitude, which is experienced by a structure in an impact scenario, as well as to determine its significance. On this basis it is investigated, whether potential influences on load magnitude follows patterns, which we can relate to ice geometry parameters, namely: cone angle, specimen length and initial contact area. To do so, a systematic investigation of different ice shapes in drop tower experiments against a rigid structure was carried out and analyzed. The main findings are summarized in the following:

1. The failure behavior of an ice specimen in an impact scenario with a rigid plate is highly dependent on the specimen shape.
2. Two main failure behaviors were identified:

- specimens that show instant global failure by spalling or cracking and show no or only little crushing.
- specimens that show first a distinct period of crushing locally at the tip of the specimen, whereas the rest of the specimen stays intact before it globally fails by spalling or cracking.

3. The failure behavior governs the magnitude of the energy and the peak force. Specimens that show instant global failure lead to forces between 30 kN and 400 kN and show a positive linear correlation between force and absorbed energy. Specimens that show first local failure before global failure results in forces up to 75 kN.
4. The peak force shows a dependency on the initial contact area. Area-like initial contact shapes show higher forces than line- or point-like initial contact shapes. The force increases with increasing initial contact area. The same applies to energy.
5. The energy absorbed by the ice during the interaction depends on the ice specimen's sharpness. Conical specimens with higher cone angles to the horizontal showed less energy needed to crush a certain ice volume.
6. The length of the specimen only demonstrated an influence in the case of cylindrical specimens. The peak force tends to increase as the length of the cylindrical specimen decreases, which is in agreement with the findings for compressive testing of brittle materials (Hawkes and Mellor, 1970; Haynes and Mellor, 1977). However, a considerable scatter in the data is observed, leading to uncertainty regarding the observed trend.
7. The experiments showed that specimens with a large initial contact area, like a cylinder or truncated cone, are highly sensitive to the alignment. The peak force drops significantly for small misalignment of 1 or less between the top surface of the specimen to the drop hammer plate.

The experiments have demonstrated that ice failure varies depending on its shape, resulting in different load magnitudes, ranging from under 50 kN, for example in the case of the dome-shaped specimen, to over 200 kN for cylindrical specimens. As a result, accounting for the ice shape becomes paramount in vertical impact scenarios involving rigid plates. This consideration is especially crucial in numerical simulations that employ specifically defined ice shapes to obtain ice loads on ship structures. In the specific scenario of an ice impact on a rigid structure, the most detrimental ice contact shape among those considered in this research, in terms of load magnitude, is a flat contact with a cylindrical ice shape. Nevertheless, this may not necessarily be the most detrimental shape in an impact scenario involving a deformable structure, such as ship hulls. The deformation can alter the failure mode and, consequently, the peak force. A specimen shape that yields the highest loads when impacting with a rigid plate may not necessarily lead to the highest deformation when impacting with a deformable plate. Further investigations are necessary to explore this aspect, involving the analysis of loads and deformations resulting from ice impacts on deformable structures.

Disclosure

Statement: During the preparation of this work the author(s) used ChatGPT in order to improve the readability and language. After using this tool, the author(s) reviewed and edited the content as needed and take(s) full responsibility for the content of the publication.

CRediT authorship contribution statement

Franciska Müller: Writing – review & editing, Writing – original draft, Visualization, Validation, Project administration, Methodology, Investigation, Formal analysis, Data curation, Conceptualization. **Angelo Böhm:** Writing – review & editing, Writing – original draft, Visualization, Methodology, Data curation, Conceptualization. **Hauke Herrnring:** Writing – review & editing, Supervision, Funding acquisition, Data curation, Conceptualization. **Franz von Bock und Polach:** Writing – review & editing, Writing – original draft, Supervision, Resources, Project administration, Funding acquisition, Conceptualization.

Sören Ehlers: Writing – review & editing, Supervision, Project administration, Funding acquisition, Conceptualization.

Declaration of competing interest

The authors declare that they have no known competing financial interests or personal relationships that could have appeared to influence the work reported in this paper.

Data availability

Data will be available under DOI: https://doi.org/10.15480/882.9069

Acknowledgement

This work was supported by the US Office of Naval Research Global (ONRG) under NICOP Grant N62909–22-1-2019. It is stated that the funder is not responsible for any of the content of this publication. Further, the authors would like to acknowledge support from MarTERA - an ERA-NET Cofund scheme of Horizon 2020 of the European Commission - and the Research Council of Norway (Project no. 311502), the Federal Ministry for Economic Affairs and Climate Action of Germany (Project no. 03SX519B), and Department of Science and Technology of South Africa, through the HealthProp project. Publishing fees supported by Funding Programme Open Access Publishing of Hamburg University of Technology (TUHH).

Appendix A. Appendices

A.1. Wedge-shaped ice specimen

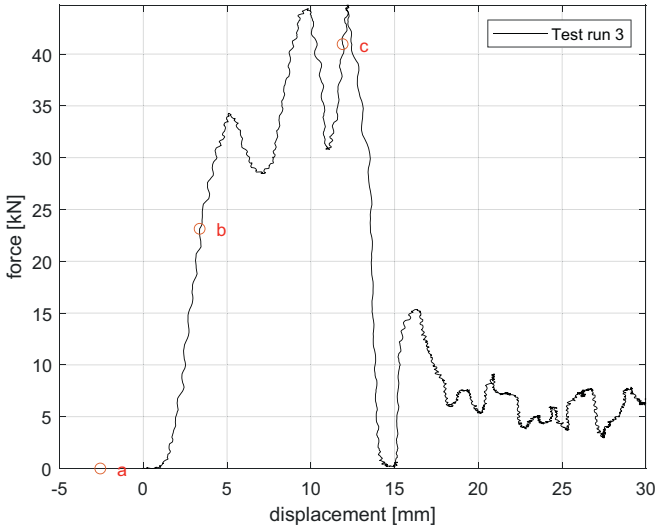

Fig. 20. Force vs. displacement plot of test run 3 of wedge shaped ice specimen. The red marked circle mark the positions of high speed footage in Fig. 21. (For interpretation of the references to colour in this figure legend, the reader is referred to the web version of this article.)

(a) intact ice specimen before contact

(b) initial local failure of top edge by crushing

(c) global failure of ice specimen by cracking

Fig. 21. Failure behavior of a wedge shaped ice specimen with 30° wedge angle.

A.2. Inclined cylinder specimen with an inclination angle of 10°

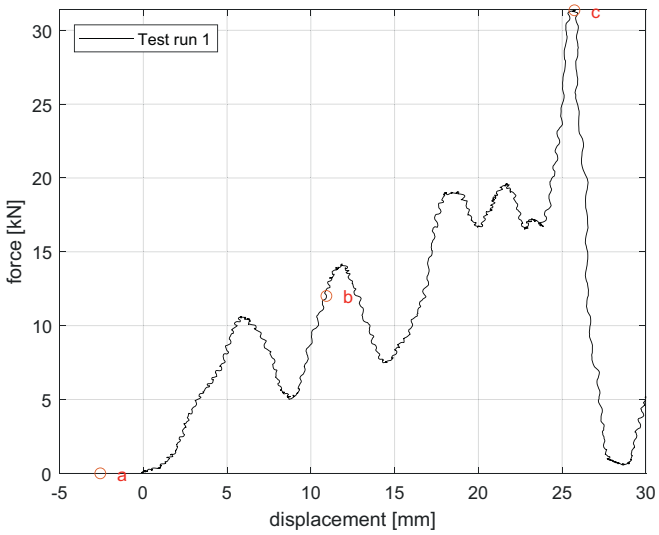

Fig. 22. Force vs. displacement plot of test run 1 of a 10° inclined cylindrical ice specimen. The red marked circle mark the positions of high speed footage in Fig. 23. (For interpretation of the references to colour in this figure legend, the reader is referred to the web version of this article.)

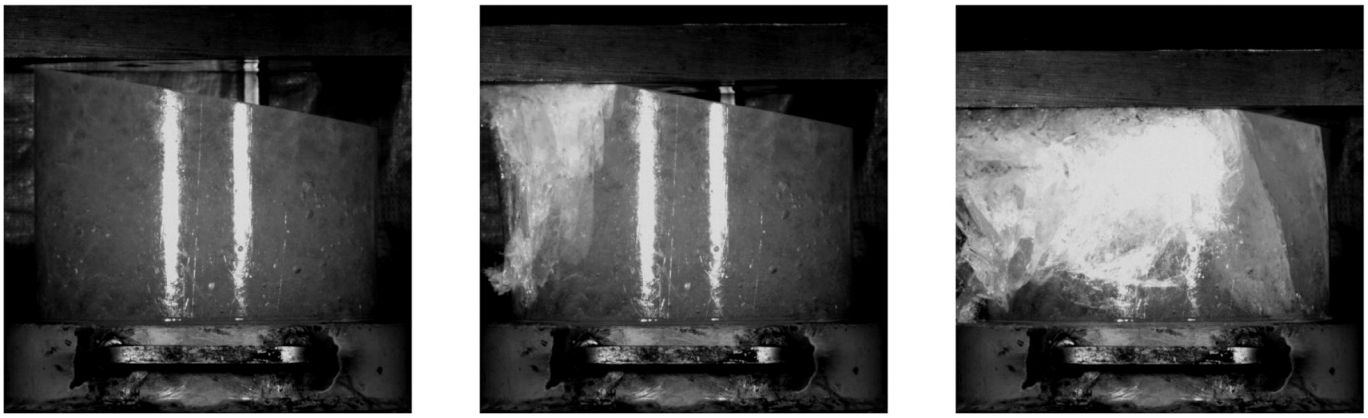

(a) intact ice specimen before contact

(b) initial local failure of ice specimen by crushing and shearing

(c) global failure of ice specimen by shearing

Fig. 23. Failure development of a cylindrical ice specimen with 10° inclined top surface. Ice specimens with 1 and 5° inclined top surface showed a similar failure behavior.

A.3. Elliptical-shaped ice specimen

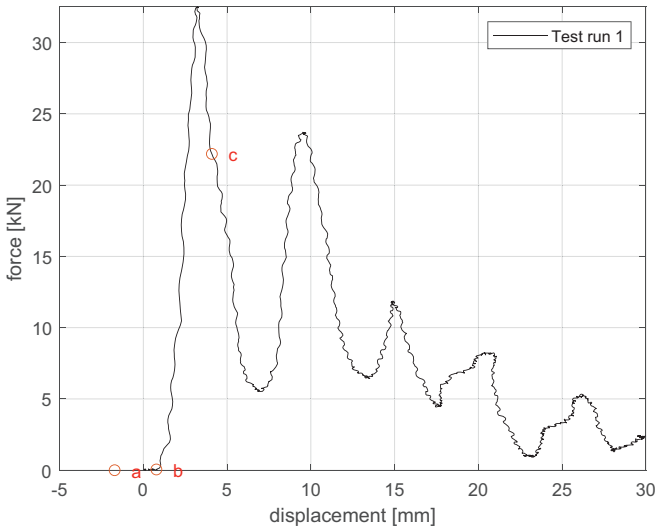

Fig. 24. Force vs. displacement plot of test run 1 of an elliptical shaped ice specimen. The red marked circle mark the positions of high-speed footage in Fig. 25. (For interpretation of the references to colour in this figure legend, the reader is referred to the web version of this article.)

(a) intact ice specimen before contact

(b) initial failure by cracking at first contact with hammer

(c) development of further cracks

Fig. 25. Failure behavior of an elliptical ice specimen. The dome-shaped ice specimen showed a similar failure behavior.

References

Allianz Global corporate & Specialty (AGCS), 2019. Safety and Shipping Review, 2019.

Allianz Global corporate & Specialty (AGCS), 2020. Safety and Shipping Review, 2020.

Allianz Global corporate & Specialty (AGCS), 2021. Safety and Shipping Review, 2021.

Böhm, Angelo Mario, Herrnring, Hauke, von Bock und Polach, Franz, 2022. Data from uniaxial compressive testing of laboratory-made granular ice. Data Brief 42, 108236.

Bruneau, S., Colbourne, B., Dragt, R., Dillenburg, A., Ritter, S., Pilling, M., Sullivan, A., 2013. Laboratory indentation tests simulating ice structure interactions using cone-shaped ice samples and steel plates. In: Proceedings of the International Conference on Port and Ocean Engineering under Arctic Conditions. POAC.

Daley, C.G., 2000. Background Notes to Design Ice Loads-Iacs Unified Requirements for Polar Ships. In: Prepared for IACS Ad-hoc Group on Polar Class Ships and Transport Canada.

Dragt, R.C., Bruneau, S.E., 2013. The collision of cone shape ice samples against steel plates of varying surface roughness. 2013. In: Proceedings of the International Conference on Port and Ocean Engineering under Arctic Conditions. POAC.

Habib, Kashfi B., Taylor, Rocky S., Jordaan, Ian J., Bruneau, Stephen, 2014. Experimental investigation of compressive failure of truncated conical ice specimens. In: Polar and Arctic Science and Technology, 10. American Society of Mechanical Engineers.

Hawkes, I., Mellor, M., 1970. Uniaxial testing in rock mechanics laboratories. Eng. Geol. 4 (3), 179–285.

Haynes, F.D., Mellor, M., 1977. Measuring the uniaxial compressive strength of ice. J. Glaciol. 19 (81), 213–223.

Herrnring, Hauke, Kubiczek, Jan M., Ehlers, Sören, 2020. The ice extrusion test: a novel test setup for the investigation of ice-structure interaction–results and validation. Ships Offshore Struct. 15 (sup1), S1–S9.

Liu, Zhenhui, Amdahl, Jørgen, Løset, Sveinung, 2011. Plasticity based material modelling of ice and its application to ship–iceberg impacts. Cold Reg. Sci. Technol. 65 (3), 326–334.

Mike Schuler gCaptain, 2023. Chinese Bulk Carrier Damaged by Ice Sinks Off Russia. https://gcaptain.com/chinese-bulk-carrier-yong-xing-56-sinks/. Accessed: 12.09.2023.

Müller, Franciska, Böhm, Angelo, Herrnring, Hauke, von Bock und Polach, Rüdiger U. Franz, Ehlers, Sören, 2023. Experimental and numerical analysis of ice crushing tests

with different shaped ice specimens. In: Polar and Arctic Sciences and Technology, 6. American Society of Mechanical Engineers.
Reddy Gudimetla, P.S., Colbourne, Bruce, Daley, Claude, Bruneau, Stephen E., 2012. Robert Gagnon. Strength and pressure profiles of conical ice crushing experiments. In: Day 2 Tue, September 18. SNAME, p. 2012.
Soares, C. Guedes, Garbatov, Y. (Eds.), 2017. Progress in the analysis and design of marine structures: Proceedings of the 6th International Conference on Marine Structures (MARSTRUCT 2017), May 8-10, 2017, Lisbon, Portugal / edited by Carlos Guedes Soares, Y. Garbatov, Boca Raton. CRC Press.
Sopper, Regina, 2016. Experimental Investigation of Water, Snow and Granular Ice Effects on Ice Failure Processes and Impact Loads.
Tuhkuri, Jukka A., Goldstein, Robert V., Osipenko, Nikolai M., 1997. Modelling of the fracture surface of an ice block failing against a structure. In: 1997 OMAE - Volume IV, 4. Arctic/Polar Technology ASME, pp. 263–269.
Zhaolong, Yu, Wenjun, Lu, van den Berg, Marnix, Amdahl, Jørgen, Løset, Sveinung, 2021. Glacial ice impacts: part ii: damage assessment and ice-structure interactions in accidental limit states (als). Mar. Struct. 75, 102889.